Real-time fluorescence and deformability cytometry

Philipp Rosendahl[1,6], Katarzyna Plak[1,2,6], Angela Jacobi[1], Martin Kraeter[1,3], Nicole Toepfner[1,4], Oliver Otto[1], Christoph Herold[1], Maria Winzi[1], Maik Herbig[1], Yan Ge[1], Salvatore Girardo[5], Katrin Wagner[1], Buzz Baum[2] & Jochen Guck[1]

[1]Biotechnology Center, Center for Molecular and Cellular Bioengineering, Technische Universität Dresden, Dresden, Germany. [2]MRC Laboratory for Molecular and Cellular Biology, University College London, London, UK. [3]Medical Clinic I, University Hospital Carl Gustav Carus, Technische Universität Dresden, Dresden, Germany. [4]Department of Pediatrics, University Hospital Carl Gustav Carus, Technische Universität Dresden, Dresden, Germany. [5]Microstructure Facility, Center for Molecular and Cellular Bioengineering, Technische Universität Dresden, Dresden, Germany. [6]These authors contributed equally to this work. Correspondence should be addressed to J.C. (jochen.guck@tu-dresden.de).

The throughput of cell mechanical characterization has recently approached that of conventional flow cytometers. However, this very sensitive, label-free approach still lacks the specificity of molecular markers. Here we developed an approach that combines real-time 1D-imaging fluorescence and deformability cytometry in one instrument (RT-FDC), thus opening many new research avenues. We demonstrated its utility by using subcellular fluorescence localization to identify mitotic cells and test for mechanical changes in those cells in an RNA interference screen.

Flow cytometry (FCM) is the gold standard for single-cell characterization in biological research and numerous clinical applications[1]. As cells flow through the cytometer, they are illuminated by lasers, and detectors collect emitted fluorescence and forward- and side-scattered light[1]. The scattered light provides information about cell morphology in the absence of a molecular label. Recently, the assessment of cells' mechanical properties has emerged as a means to obtain orthogonal information about the functional state of whole cells without labels. Importantly, cell mechanics is tightly regulated and serves as a quantitative readout for the state of the cytoskeleton[2,3]. A cell's stiffness is influenced by its progression through the cell cycle[4,5], differentiation[5,6], and pathophysiological processes such as malignant transformation[7,8] and immune-cell activation[9–11]. With the recent advent of several microfluidic techniques and their massive increase in throughput (~100–10,000 cells per second), mechanical phenotyping can now be performed at rates of conventional FCM[5,12,13]. Among many other applications, this opens up the possibility of large-scale screening for genes that regulate cell mechanics, which was previously limited by the low throughput (~10–100 cells per hour) of techniques such as atomic force microscopy.

Label-free approaches provide quantitative information about cells but lack molecular specificity, which can be achieved in principle through the use of fluorescent probes[1]. The total amount of a certain fluorescent probe in a cell is what is usually quantified in standard FCM. More advanced variants of FCM, such as fluorescence pulse-shape analysis[14] and slit-scanning[15], and the use of line-scan cameras[16] and nonlinear optics[17] can even provide the 1D and 2D intracellular distribution of fluorescence, respectively. The combination of the molecular specificity of such FCM analysis with mechanical phenotyping, which is very sensitive to changes in cell state, promises to open up entirely new possibilities for scientific exploration.

Here we present RT-FDC, which combines 1D-resolved, fluorescence-based FCM with mechanical phenotyping for the continuous analysis of large cell populations (**Fig. 1a**). The principle of operation is based on real-time deformability cytometry (RT-DC)[5]. Up to 100 cells per second are flowed through a microfluidic chip (**Supplementary Fig. 1**) and deformed without physical contact by hydrodynamic interactions in a constriction zone[18,19] (**Fig. 1b**). Stroboscopic high-speed bright-field microscopy with real-time image processing captures and evaluates the cell contour. Simultaneously, three diode lasers excite fluorescence in a light sheet perpendicular to the channel axis (**Fig. 1a**, **Supplementary Fig. 2a–c**), and avalanche photodiode detectors measure emitted fluorescence intensity in the region. We checked the synchronicity of the different fluorescence channels, using custom-made two-color fluorescent agarose beads (**Supplementary Fig. 2d**). If an object is detected in the bright-field image, the custom algorithm extracts the cross-sectional area and deformation (**Fig. 1b**), which can be related to the object's elastic modulus[18,19], and analyzes the respective fluorescence signal for peak maximum, width, and area. We confirmed that fluorescence detection by RT-FDC is comparable to that of standard FCM with calibration beads (**Supplementary Fig. 3**). To test the utility of RT-FDC for biological and biomedical research, we assessed the mechanical properties of fluorescently labeled subpopulations of cells in a heterogeneous mixture without prior sorting.

Surface marker labeling is the standard approach for identification of many different cell types, including hematopoietic stem and progenitor cells (HSPCs)[5]. Previous studies have shown that mechanical properties of HSPCs are linked to their circulation and migration abilities[6,20]—essential aspects of successful HSPC homing when the cells are used for transplantation after chemotherapy. To test whether cell mechanics can be used as a phenotypic marker for human CD34$^+$ HSPCs, we measured the mechanical properties of cells from granulocyte colony-stimulating factor (G-CSF)-mobilized peripheral blood. After

classifying the cells into CD34$^+$ and CD34$^-$ subpopulations on the basis of fluorescence intensity by RT-FDC (**Fig. 1c**), we obtained the mechanical fingerprint (deformation versus area; **Fig. 1d,e**), which showed that CD34$^+$ cells had a mean size of 61.1 ± 1.3 µm^2 and low deformation (0.02–0.05), corresponding to an elastic modulus of ~1 kPa; we confirmed these findings with cells from three different donors. For outliers in the CD34$^+$ population there was no correlation between CD34 expression and deformation or projected area (**Supplementary Fig. 4**). Compared to the CD34$^+$ fraction, CD34$^-$ cells were either smaller (lymphoid cells)[5,11] or larger (monocytes and granulocytes)[5,11] and had a wider distribution in deformation. An exemplary multicolor analysis excluding T cells and monocytes and using specific lineage markers is shown in **Supplementary Figure 5**, and validates antibody-based identification of HSPCs. We also tested the potential for sorting cells by deformation and cell size, without relying on fluorescence. Assuming the fluorescence readout represented the ground truth, we found that classification by mechanical fingerprint (**Fig. 1d**) yielded sensitivity of 69.1% and specificity of 90.9% (**Supplementary Table 1**). The prevalence was 0.55%, as confirmed by FCM (**Supplementary Fig. 6**). Importantly, this would be sufficient to enrich for HSPCs in G-CSF mobilized blood on the basis of their morphological and mechanical phenotype alone. As a second test case, to demonstrate the applicability of RT-FDC with cell-permeant fluorescent dyes, we used RT-FDC to determine the mechanical properties of mature red blood cells (RBCs) compared with those of immature reticulocytes (**Supplementary Fig. 7**, **Supplementary Table 2**). Reticulocytes were slightly larger and less deformed compared with RBCs.

In addition to detecting total fluorescence intensity, the setup also permits 1D fluorescence imaging. When cells in the channel pass through the light sheet (3-µm thickness; **Supplementary Fig. 2a–c**) at a constant speed, the temporal shape of the fluorescence peak provides a measure of the subcellular distribution of fluorophores in the channel direction (**Supplementary Fig. 2a**). This enables RT-FDC to provide spatial information about the localization of fluorescence signal within cells (**Supplementary Fig. 8**). We exploited this possibility to screen for changes in cell mechanics that accompany entry into mitosis in the *Drosophila* cell line Kc167. Mitotic cells, which represent ~5% of an asynchronous population of proliferating cells, were detected on the basis of nuclear envelope breakdown— characterized by the entry of nuclear localization signal (NLS)–GFP into the cytoplasm, which equalized the GFP and tdTomato peak widths (**Fig. 2a**, **Supplementary Fig. 9**)—and their specific mechanical fingerprint was analyzed (**Fig. 2b**). This enabled us to use RNA interference in combination with RT-FDC to investigate the mechanical effects of 42 genes

chosen for their function as regulators of the cortical actin cytoskeleton in mitotic cells. The detailed analysis pipeline and all screening results can be found in **Supplementary Figures 10** and **11**, **Supplementary Table 3**, and the **Supplementary Discussion**. This screen identified a set of both known and novel genes involved in the regulation of mitotic cortical mechanics, revealing important roles for Rho GTPase-activating proteins in opposing the activity of the mitotic Rho guanine nucleotide-exchange factors (primarily Ect2/Pbl). Thus, RT-FDC makes it possible to screen for regulators of cell mechanics in small subpopulations of cells. Of note, the conventional, two-color FUCCI cell cycle probe also can be used with RT-FDC. However, only through the 1D fluorescence-localization capabilities of RT-FDC can G2- and M-phase cells be distinguished and mechanical differences between mitotic and interphase cells be identified (**Supplementary Figs. 12** and **13**).

We were also able to identify intracellular structures smaller than the nucleus, such as separating chromatids during mitosis in cells carrying fluorescently labeled histone 2B (**Fig. 2c,d**). In this way HeLa cells could be separated into metaphase and anaphase populations on the basis of the presence of single and double peaks of mCherry fluorescence signal, respectively. An important aspect for the detection of separated chromatids is the proper alignment of cells, which are elongated along the spindle axis, with the channel axis, which is ensured by the hydrodynamic forces acting on the elongated cells.

The combination of the molecular specificity of fluorescent probes with the sensitivity of the measured cell mechanics as a functional readout in RT-FDC enables correlation of both, or gating for rare cells in large samples for mechanical analysis. In the future, the possibility to enrich for cells by using mechanics alone might aid or even replace the current label-based purification of cells, which might be particularly interesting for clinically relevant cells such as HSPCs. Our results further show that the technique is ideal for screening for regulators of cell mechanics. Screens focused on mechanical properties will benefit from the high throuput per sample (100 cells per second), as well as from the short time needed to complete one experiment (15 min), which allowed us to carry out more than 500 individual measurements in the presented screen for candidate genes involved in the regulation of cell mechanics during mitosis. Future investigations of mitotic cell mechanics could take into account information encoded in the fluorescence peak with greater detail, as demonstrated for H2B HeLa cells for resolution of meta-, ana-, and telophase. This aspect highlights the need for simultaneous fluorescence and mechanical readout: if cells had to be presorted before mechanical measurement by any given method, time-sensitive phases, such as mitosis, could not be resolved because of the experimental delay. Only simultaneous readout retrieves the

full information at the single-cell level, going beyond the state of the art of what is achievable with FCM or deformability cytometry alone.

METHODS

Methods, including statements of data availability and any associated accession codes and references, are available in the online version of the paper.

Note: Any Supplementary Information and Source Data files are available in the online version of the paper.

AUTHOR CONTRIBUTIONS

J.G. conceived the project. P.R. built the experimental setup. O.O. and C.H. supported the optics design. P.R. programmed the real-time data-evaluation software. K.P. designed and performed experiments on Kc167 and HeLa cells and analyzed the data with B.B.'s support. P.R. and N.T. performed experiments with RBCs. A.J., M.K., and P.R. performed experiments on HSPCs and analyzed the data. P.R. performed and analyzed experiments for device characterization. M.H., O.O., and Y.G. developed the linear mixed model algorithm for statistical evaluation. K.W. and S.G. produced fluorescent beads for device characterization. M.W. performed reference measurements with calibration beads on FCM. S.G. produced masters for microfluidic chips. J.G. and B.B. supervised the project. P.R., K.P., and J.G. wrote the manuscript. All authors reviewed the manuscript.

COMPETING INTERESTS

P.R., O.O., and C.H. are shareholders and employees of the company Zellmechanik Dresden GmbH, which sells devices based on RT-DC and RT-FDC technology. All other authors declare no competing interests.

1.   Shapiro, M.H. *Practical Flow Cytometry* (John Wiley & Sons, Inc., 2003).

2.   Elson, E.L. *Annu. Rev. Biophys. Biophys. Chem.* **17**, 397–430 (1988).

3.   Fletcher, D.A. & Mullins, R.D. *Nature* **463**, 485–492 (2010).

4.   Matthews, H.K. *et al. Dev. Cell* **23**, 371–383 (2012).

5.   Otto, O. *et al. Nat. Methods* **12**, 199–202 (2015).

6.   Ekpenyong, A.E. *et al. PLoS One* **7**, e45237 (2012).

7.   Tse, H.T.K. *et al. Sci. Transl. Med.* **5**, 212ra163 (2013).

8.   Guck, J. *et al. Biophys. J.* **88**, 3689–3698 (2005).

9.   Worthen, G.S., Schwab, B.I., Elson, E.L. & Downey, G.P. *Science* **245**, 183–186 (1989).

10.   Bufi, N. *et al. Biophys. J.* **108**, 2181–2190 (2015).

11.   Toepfner, N. *et al. eLife* **7**, e29213 (2018).

12.   Gossett, D.R. *et al. Proc. Natl. Acad. Sci. USA* **109**, 7630–7635 (2012).

13.   Nyberg, K.D. *et al. Biophys. J.* **113**, 1574–1584 (2017).

14.   Ramdzan, Y.M. *et al. Nat. Methods* **9**, 467–470 (2012).

15.   Gray, J.W., Peters, D., Merrill, J.T., Martin, R. & Van Dilla, M.A. *J. Histochem. Cytochem.* **27**, 441–444 (1979).

16.   Basiji, D.A., Ortyn, W.E., Liang, L., Venkatachalam, V. & Morrissey, P. *Clin. Lab. Med.* **27**, 653–670 (2007).

17.   Lau, A.K.S., Shum, H.C., Wong, K.K. & Tsia, K.K. *Lab Chip* **16**, 1743–1756 (2016).

18.   Mietke, A. *et al. Biophys. J.* **109**, 2023–2036 (2015).

19.   Mokbel, M. *et al. ACS Biomater. Sci. Eng.* **3**, 2962–2973 (2017).

20.   Kräter, M. *et al. Sci. Rep.* **7**, 2549 (2017).

Figure 1 | Real-time fluorescence and deformability cytometry. (**a**) Experimental setup. Cells are pumped through a microfluidic channel and imaged by bright-field microscopy, while three lasers excite and avalanche photodiodes measure fluorescence. (**b**) In the narrow constriction zone, cells deform as a result of hydrodynamic interaction, and deformation is

determined by image processing. Focused lasers excite fluorescence in the region marked in yellow (**c–e**) HSPCs were surface-labeled with anti-CD34 conjugated to allophycocyanin (APC). (**c**) Log histogram of CD34–APC fluorescence, and gate used for classification. (**d**) CD34$^+$ cells form a homogeneous population. The color-coding corresponds to a linear density scale, as indicated by the key. The black outline around the cell cluster represents the gate used to calculate the confusion matrix. (**e**) The plot of deformation versus area for CD34$^-$ cells shows more spread than that for CD34$^+$ cells. Experiments were repeated three times, with similar results each time.
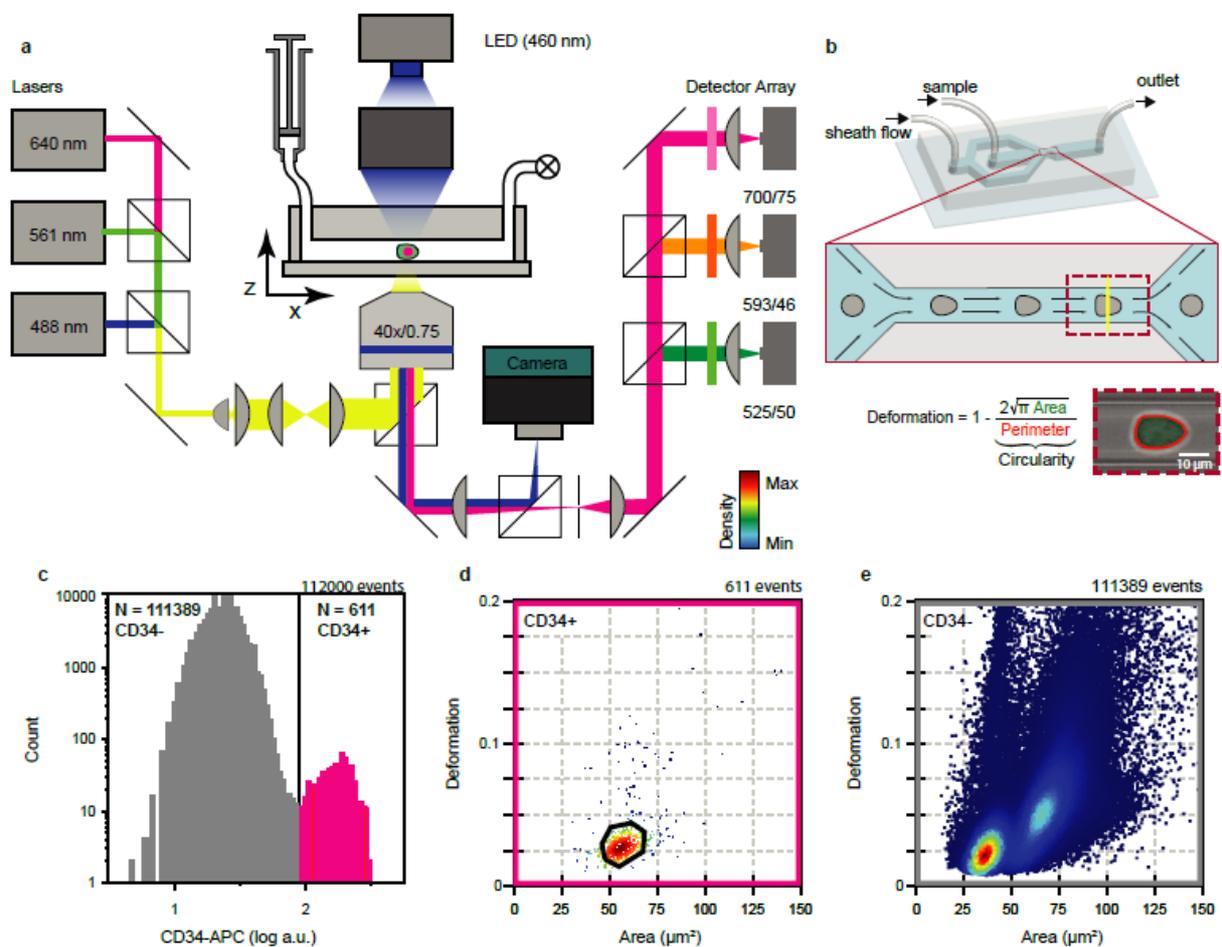
Figure 2 | 1D fluorescence imaging for identification of mitotic cells. (**a**) Nuclear envelope breakdown leads to equal peak widths for NLS–GFP and tdTomato. Mitotic cells along the diagonal can be gated by the red outline (**Supplementary Fig. 9** Interphase cells are shown in gray, while mitotic cells are colored according to a linear density scale. (**b**) Deformation versus area of the mitotic subpopulation. Results in **a,b** are from one experiment

representative of three repeated experiments. (**c,d**) Subcellular localization of H2B–mCherry in HeLa cells. Cells in (**c**) metaphase and (**d**) anaphase exhibited one or two fluorescence peaks corresponding to one metaphase plate (arrow in **c**) or two separated chromatids in the bright-field images (arrows in **d**), respectively. Experiments in **c,d** were performed five times independently, with similar results each time. a.u., arbitrary fluorescence units.
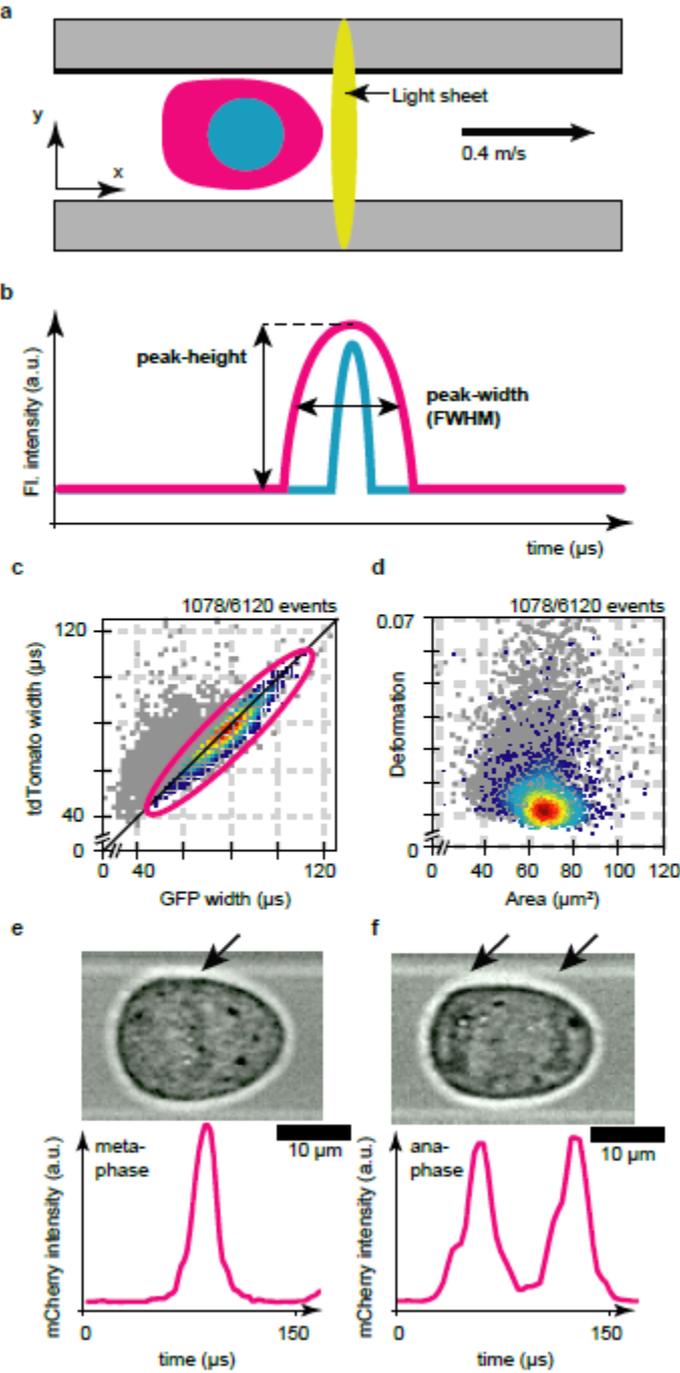
ONLINE METHODS

Experimental setup.

Figure 1 shows the overall experimental setup used throughout this study. The microfluidic chip, synchronized pulsed LED illumination (AcCellerator L1; Zellmechanik Dresden), syringe pump (neMESYS; Cetoni), and bright-field imaging (MC1365; Mikrotron) were adapted from RT-DC as described previously[5]. **Supplementary Figure 14** provides additional technical details about the excitation and emission light paths too small to see in **Figure 1**. For fluorescence excitation, three solid-state lasers (OBIS 488-nm LS 60 mW; OBIS 561-nm LS 50 mW; OBIS 640-nm LX 40 mW; Coherent Deutschland) in combination with adjustable mounted dichroic mirrors (561-594R, 473-491R, and 1064R; Semrock) create a combined beam. This aspect is particularly difficult to achieve and requires advanced optics skills; the use of a shearing interferometer is beneficial. The beam is expanded and collimated by two achromatic lenses (AC080-010-A-ML and AC254-040-A-ML; Thorlabs) and then focused to a sheet in the image plane of the microscope with a cylindrical lens (LJ1695RM-A; Thorlabs). The position and angle of this cylindrical lens have to be aligned carefully to focus the light sheet in the object plane of the objective. Alignment success can be checked best with a fluorescent sample, such as a text marker line on a thin microscope slide. Excitation light is coupled into the microscope (Axio Observer.Z1; Carl Zeiss Microscopy) through the modified backport for epifluorescence illumination. Below the 40× objective (EC Plan-NEOFLUAR 40×/0.75-NA (numerical aperture); Carl Zeiss Microscopy), a QuadLine beam splitter (zt405/488/561/640rpc; Chroma Technology) reflects excitation light toward the specimen but transmits light emitted by the sample to the detector assembly. A second beam splitter (zt 473 RDCXT; Chroma Technology) separates light from the LED illumination with 460 nm to the CMOS (complementary metal-oxide semiconductor) camera (MC1365; Mikrotron) for bright-field imaging, which has a quantum efficiency of about 30% in this spectral band and operates at frame rates up to 4 kHz for our application. Light of longer wavelengths is directed to an adjustable slit (VA100C/M; Thorlabs) that is in the image plane of the microscope and part of the confocal detector assembly. The collimated beam is separated into three fluorescence channels—FL-1 (FF555-Di03, FF03-525/50; Semrock), FL-2 (zt 633 RDC, Chroma Technology Corp; FF01-593/46, Semrock), and FL3 (700/75 ET; Chroma Technology Corp)—and finally focused (LA1951-A-ML; Thorlabs) on the three avalanche photodiode detectors (MiniSM10035; SensL Corporate).

The analog detector signals are digitized by a PCIe (peripheral component interconnect express) card (NI PCIe-6531; National Instruments Germany) at a sample rate of

1 MHz (shared between channels) and stored in a circular buffer of 1,000,000 samples for real-time analysis. Because the trigger signal for image acquisition is derived from the same clock as the detector data acquisition, the image and fluorescence acquisition are synchronized. If an object is detected in an image, the corresponding part of the detector signal is fetched from the circular buffer and also analyzed. For image processing, we used the OpenCV 3.1 computer vision library (http://opencv.org) wherever possible. Image processing included the following steps: subtraction of a background image (rolling average of the last 100 camera images), threshold operation, finding contours in the binary image via a border-following algorithm[21], determining particle cross-sectional area, deformation (1 – circularity) and position of the contour. Additionally, the mean brightness of pixels inside the contour is determined along with the s.d. In case these parameters match the gates set before, the corresponding fluorescence detector signal is fetched from the circular buffer and analyzed for the maximum value, the peak width (full-width at half-maximum (FWHM)), the peak area, and the peak position. These parameters are stored together with results from image processing, an image of the cell, and the fluorescence peak on the disk of the computer for later analysis and are instantly plotted on the screen.

For characterization of the aperture function (sensitivity as a function of position), 3-µm fluorescent beads (BD FACSDiva CS&T Research Beads; Becton Dickinson) were embedded in 1% agarose gel (low gelling temperature A0701-100G; Sigma-Aldrich) on a microscope slide (Thickness 2; Glaswarenfabrik Karl Hecht) and moved through the detection volume on the automated microscope stage while the detector signals were recorded to obtain the combined fluorescence excitation and emission efficiency for a field of 30×60 µm as shown in **Supplementary Figure 2b**. Because the microscope slide was the same as that used for the microfluidic chips and the refractive index of 1% agarose gel is very close to that of water ($n = 1.34$), we assumed that the light sheet in the microfluidic channel and the bead test slide had very similar shapes. The resulting thickness of the light sheet (FWHM) along the channel axis is presented in **Supplementary Figure 2c** and was about 3 µm for all fluorescence channels. This is also the size of the fluorescent bead and thus highlights the capability of the device to detect localization of fluorophores in cell compartments such as the nucleus that have a size of about 5 µm.

The dynamic range of the fluorescence detection system was tested with flow cytometer calibration beads (Spectral calibration PMMA beads; PolyAn; lot FP170601A). As expected, eight populations showed up in the histogram of the fluorescence peak heights (**Supplementary Fig. 3**), in agreement with reference measurements provided in the

manufacturer's manual and our own measurements obtained on an LSR II flow cytometer (Becton Dickinson). Fluorescence peak width detection in different channels is compared in **Supplementary Figure 2d**, which shows data from two-color fluorescent agarose beads with heterogeneous sizes. These beads were produced from a mixture of two ultra-low-gelling-point agarose solutions, one functionalized with Alexa Fluor 488, the other with Alexa Fluor 633. For cross-linking we decreased the temperature below the gelling point, which resulted in stable beads that could be stored for weeks. The linear fit showed that the peak widths in the green and the red channels (FL-1 and FL-3) were proportional, with a slope close to 1 and a small offset of –0.1 µs, demonstrating that peak-width measurements can be compared across channels for investigations of fluorophore localization (**Supplementary Fig. 2d**). The particle speed in the flow for this measurement was about 0.4 m s^{-1}, so the particle diameters ranged from 5 µm to 35 µm based on the fluorescence signal peak widths. All the setup characterization experiments consisted of three technical repeats.

Experimental procedure.

For all experiments, cells or micro-particles were suspended in phosphate-buffered saline without magnesium or calcium (PBS$^-$) complemented with 0.5% or 0.6% (w/v) methylcellulose (Alfa Aesar) to slow down sedimentation during the experiment. The methylcellulose solution was calibrated with a falling-ball viscometer (Haake Typ C; Thermo Fisher Scientific) to a viscosity of 15.0 ± 0.8 mPa·s and 25 ± 0.6 mPa·s at 24 °C for 0.5% and 0.6% methylcellulose, respectively. Prior to the experiments, the cell suspension was aspirated into PEEK tubing (Upchurch; Thermo Fisher Scientific) connected to a 1-mL plastic syringe (Becton Dickinson) at a flow rate of 1 µl s^{-1}, avoiding high stress on the specimen. Then the tubing was connected to the microfluidic chip (**Fig. 1b**, **Supplementary Fig. 1**), where constant flow was generated by a combination of sheath and sample flow with a ratio of 3:1. After equilibration of the flow for 2 min, the measurement was started. The camera's region of interest (256 × 96 pixels) was positioned at the end of the 300-µm-long channel region of the chip to ensure cell deformation had reached a steady state. Laser powers can be adjusted in the range of 1–60 mW to match the detector's dynamic range in an optimal way. Because of the low spectral overlap between fluorophores used in our experiments, no compensation was applied to raw fluorescence data. Compensation procedures may, however, be performed according to standard methods. Depending on the cell concentration in the sample, measurements ran for one to a few minutes and yielded typically 2,000–100,000 events at rates of up to 100 events per second. Higher throughput rates were not possible because multiple cells in the image might impede the correct assignment of fluorescence

peaks to cells in the image data. Post-experimental data analysis was performed with the following programs: ShapeOut (Zellmechanik Dresden; https://github.com/ZELLMECHANIK-DRESDEN/ShapeOut) for plotting and gating, and OriginPro 9.0 (OriginLab Corporation) for more detailed data inspection, plotting, and fitting.

Hematopoietic stem cell isolation and preparation.

With approval for the study (EK221102004) from the ethics committee of the Technische Universität Dresden, we analyzed the apheresis product from G-CSF-mobilized peripheral blood from three healthy human donors, obtained with their informed consent in accordance with the guidelines of good practice and the Declaration of Helsinki. Before measurement by RT-FDC, HSPCs were stained for 30 min with anti-CD34–APC (555824; Becton Dickinson), then pelleted by centrifugation ($200g$, 5 min, 23 °C and resuspended in 0.6% methylcellulose solution.

Reticulocyte and red blood cell preparation.

With approval for the study (EK89032013) from the ethics committee of the Technische Universität Dresden, we obtained blood from three healthy donors with their informed consent in accordance with the guidelines of good practice and the Declaration of Helsinki. Capillary blood was collected by finger prick with a 21-gauge, 1.8-mm safety lancet (Sarstedt). For sample preparation, 2 µL of blood was diluted in 1 mL of 0.5% methylcellulose solution complemented with 2.5 µM syto13 nucleic acid stain (Thermo Fisher Scientific). We measured cells from three healthy donors after 5 min of incubation; measurements usually took 10 min. To validate the stability of mechanical phenotype and fluorescence staining in methylcellulose measurements, we used a 1-h time course with measurements every 10 min for all donors. To validate counting results, we collected blood from venipuncture with a 21-gauge needle (Multifly; Sarstedt) in EDTA (S-Monovette 1.4 mL 9NC; Sarstedt) for measurements with RT-FDC and parallel full blood counts on a state-of-the-art device (XE-5000; Sysmex Deutschland) at the Institute for Clinical Chemistry and Laboratory Medicine at the Carl Gustav Carus University Hospital, Technische Universität Dresden.

Cell lines and culture.

The stable H2B–mCherry HeLa cell line was kindly provided by the lab of Matthieu Piel (Institute Curie). All HeLa cells were grown in standard DMEM supplemented with 10% FBS and 2 mM L-glutamine. Transfection of HeLa cells was done with Effectene reagent (Quiagen) according to the manufacturer's directions. We allowed cells to grow for 48 h after

transfection, and we removed dead cells by washing away loosely attached cells. Prior to RT-FDC measurements, adherent cells were trypsinized, collected by centrifugation (200g, 5 min, 23 °C and resuspended in 0.5% methylcellulose buffer.

For mitotic synchronization of the H2B–mCherry HeLa line, cells were allowed to grow to 35% confluence and were then synchronized with 100 nM nocodazole for 5 h. Mitotic cells were collected by shake-off, and nocodazole was washed away. Cells were then allowed to progress through mitosis in full media for 15 min (metaphase cells) or 1 h (anaphase cells).

Kc167 *Drosophila* cells were grown in M3 Shields and Sang medium supplemented with 10% FBS. For detection of mitotic cells, we engineered a stable Kc167 cell line that expresses tdTomato cytosolic protein and NLS(GFP)2(GST), a protein that stably localizes to the nucleus during interphase. At the entry to mitosis, the nuclear envelope breaks down and the nuclear GFP signal is redistributed to the cytoplasm, where it colocalizes with tdTomato. Analysis of fluorescence peak widths distinguished interphase cells (narrow GFP peak and broad tdTomato peak) from mitotic cells (both peaks of the same width; **Fig. 2c**). Owing to progression through mitosis and cytokinesis, cells in late mitotic stages have nonspherical shapes due to elongation and furrow constriction before division (anaphase and telophase of mitosis), which can bias the deformation readout of RT-FDC. To avoid this effect, we focused on prometaphase cells by synchronization with colchicine, a drug that inhibits formation of the mitotic spindle. Cells were synchronized with 4 µM colchicine for 5 h for enrichment of the mitotic cell fraction (**Supplementary Fig. 9**). RNA interference experiments were conducted as described[22]. The treatment with colchicine led to an increase in mitotic cell size; however, it did not affect the mechanical phenotype of mitotic cells (**Supplementary Table 4**) and, as expected, it led to enrichment of the mitotic cell fraction (**Supplementary Fig. 9**).

RNA interference screening.

For each of the 42 candidate genes (**Supplementary Table 5**), RNA interference was performed with two nonoverlapping double-stranded RNA sequences. Data from three independent experiments performed on different days were collected for each RNA sequence and compared with data for negative controls acquired on the same day (**Supplementary Fig. 11**). For evaluation of the measured elastic modulus values, a linear mixed model (LMM)[23] comparison was performed with the software ShapeOut (Zellmechanik Dresden), for which data for each gene (different days, different sequences) were pooled. We rejected the null model on the basis of a P value < 0.05 as a hit. Only if the effect was visible for both flow

rates (0.04 and 0.06 µL s^{-1}) was the gene considered to play a role in the regulation of mitotic cell mechanical properties.

Statistical analysis.

Statistical analysis was done via the LMM method integrated into ShapeOut. The method is described in detail in ref. 23. LMM evaluation was necessary to take into account random variations of the mean values between replicates caused by variables that are not controlled by the experimenter. We defined and fitted an LMM using the R package "lme4"[24,25]. To test the null hypothesis, we fitted a model with and without the fixed effect term and compared the two models by a likelihood test[26]. From the resulting likelihood ratio, one can compute the *F*-value and *P* value by using Wilks theorem[27].

Code availability.

The source code of ShapeOut, the program used to analyze and plot the RT-FDC data, is open source and can be found on GitHub (https://github.com/ZELLMECHANIK-DRESDEN/ShapeOut). The source code for the custom C++ acquisition software is available from the corresponding author upon reasonable request.

Life Sciences Reporting Summary.

Further information on experimental design is available in the **Life Sciences Reporting Summary**.

Data availability.

The data that support the findings of this study, as well as general information and biological materials, are available from the corresponding author upon reasonable request. The raw RT-FDC data are available as TDMS files that can be read, processed, and analyzed by ShapeOut. Polygon filters used to select the cell populations of interest are available upon request and are also compatible with the ShapeOut software. Source data for **Figures 1** and **2** are available online.

21.   Suzuki, S. *Comput. Vis. Graph. Image Process.* **46**, 32–46 (1985).

22.   Baum, B. & Cherbas, L. *Methods Mol. Biol.* **420**, 391–424 (2008).

23.   Herbig, M. *et al.* in *Flow Cytometry Protocols* (eds. Hawley, R. & Hawley, T.) 347–370 (Humana Press, 2017).

24.   R Core Team. *R: A Language and Environment for Statistical Computing* (R Foundation for Statistical Computing, 2015).

25.   Bates, D. *R News* **5**, 27–30 (2005).

26.   Mood, A.M., Graybill, F.A. & Boes, D.C. *Introduction to the Theory of Statistics* 3rd ed. 540–541 (McGraw-Hill, 1974).

27.   Wilks, S.S. *Annals of Mathematical Statistics* **9**, 60–62 (1938).